DOI: 10.1002/ente.201500014

Transparent Metal Network with Low Haze and High Figure of Merit applied to Front and Back Electrodes in Semitransparent ITO-free Polymer Solar Cells

Christoph Hunger,[a] K. D. M. Rao,[b] Ritu Gupta,[b] Chetan R. Singh,[a] Giridhar U. Kulkarni,*[b] and Mukundan Thelakkat*[a]

In the quest for indium-tin oxide (ITO)-free photovoltaics and for building integrated as well as automobile roof applications, novel transparent electrodes for both front and back electrodes are required. Here we report the fabrication and integration of submicrometer transparent silver (Ag) and gold (Au) metal network electrodes, which are invisible to the naked eye, in organic photovoltaic devices. We exploit the idea of using the spontaneous cracking of a polymer layer as template to prepare the metal network. The main challenge is to apply the cracked template approach on top of soluble organic layers and to lift off the template without damaging the photoactive layer. We demonstrate that Ag or Au back electrodes can be fabricated maintaining a transmittance of 80% for the whole visible range. These electrodes exhibit ultralow haze of approximately 5% and an excellent figure of merit value. Moreover, the ITO-free semitransparent polymer solar cell incorporating the Ag/Ag network electrodes exhibits 57% transmittance above 650 nm.

Introduction

Solution-processed organic solar cells have made rapid progress towards technology as a potential source of deriving solar energy in recent years.[1,2] The major part of research on organic solar cells was in terms of design and development of efficient photoactive materials with new acceptor and donor moieties to improve the power conversion efficiency (PCE).[3,4] However, the quest for efficient, scalable and rational processing methods for both active layers and electrodes has gained momentum towards application-specific requirements such as large-area processing, low weight, semitransparency, and mechanical resilience for future photovoltaics technologies such as electronic skin, textiles, and building integrated photovoltaics (PV).[1,2,5] Here we address the questions concerning the fabrication of indium-tin oxide (ITO)-free electrodes and how to achieve semitransparency in polymer solar cells using these novel electrode materials.

In most organic solar cells, ITO serves as a transparent conducting front electrode (TCE) whereas opaque metal films (such as Ag, Au, or Al) are used as back electrodes. ITO is known for its high transparency, reaching approximately 90% in the visible region, and low sheet resistance of 10 Ω/□.[6] But ITO is also scarce and expensive[7] and requires high-temperature processing as well as being brittle so that cracks develop on flexible substrates.[8] Therefore TCE alternatives based on graphene,[9] carbon nanotubes,[10,11] Ag nanowires (NWs),[12,13] or printed current-collecting grids from Ag paste[14,15] have been developed to replace ITO. Graphene and carbon nanotubes exhibit high transparencies, comparable to ITO, but they suffer from high contact resistances.[9,10] However, TCEs made from Ag NWs have both high transparency (90% in the visible region) and a sheet resistance as low as 20 Ω/□.[16] To keep the sheet resistance low, a relatively thick layer of well-connected Ag NWs is essential and the layer needs further treatments such as pressing or nano-welding.[17] Printed collecting grids fabricated from Ag paste do not have such problems, but as the dimensions of the printed Ag grid are usually in the range of 200–300 μm, it is visible to the naked eye and therefore not ideal as semitransparent electrode in building-integrated or automobile roof photovoltaic applications.[2,16]

One big advantage of organic solar cells with respect to their inorganic counterparts is the semitransparency as well as the color tunability of their photoactive layer. To make the entire solar cell semitransparent, not only the front electrode but also the back electrode need to be transparent. To achieve this, most of these semitransparent solar cells use ITO as front electrode and Ag NWs as back electrode. The Ag NWs itself are filled or blended with PEDOT:PSS, MoO_3, ZnO, or ITO particles to yield a PCE of 2–2.5% for P3HT:PCBM blends.[18,19] Another possibility for a transparent back electrode is based on an ultrathin metal layer. Chen et al. demonstrated semitransparent solar cells with the help

[a] C. Hunger, Dr. C. R. Singh, Prof. Dr. M. Thelakkat
Applied Functional Polymers, Macromolecular Chemistry I
University of Bayreuth
95440 Bayreuth (Germany)
E-mail: mukundan.thelakkat@uni-bayreuth.de

[b] Dr. K. D. M. Rao, Dr. R. Gupta, Prof. Dr. G. U. Kulkarni
Chemistry & Physics of Materials Unit and Thematic Unit of Excellence in Nanochemistry
Jawaharlal Nehru Centre for Advanced Scientific Research
Jakkur P.O., Bangalore 560 064 (India)
E-mail: kulkarni@jncasr.ac.in

Supporting information for this article is available on the WWW under http://dx.doi.org/10.1002/ente.201500014.

of an ultrathin Ag layer as back electrode and a low-band-gap (LBG) Polymer/$PC_{[71]}BM$ as photoactive layer.[20] Here, the thickness of the metal layer needs to be very small (< 10 nm) to guarantee adequate transparency, which is usually achieved at the cost of conductivity.

There are only a few ITO-free semitransparent polymer solar cells reported in literature. The first report involves the use of PEDOT:PSS both as front and back electrodes resulting in a PCE of 0.5% for the P3HT/$PC_{[61]}BM$ System.[21] On the other hand, a combination of Ag NWs and PEDOT:PSS led to PCEs ranging from 2.0 to 2.3% for polymer solar cells containing P3HT as donor.[22,23] Very recently a similar electrode combination was also demonstrated for a LBG polymer/PCBM device.[24] But, it has been demonstrated that metal network electrodes based on cracked templates with network widths ranging from several hundreds of nanometers up to 5 μm can be developed and integrated into electronic devices as replacements for ITO.[25–27] The major advantages of these submicrometer metal network electrodes are their high transmittance and very low sheet resistances. Additionally, this template method is highly scalable. Furthermore, the crack template can be used not only for Ag or Au, but for any metal to form the respective network. However, these metal network electrodes had not been fabricated on top of an organic layer up to now. Moreover its applicability to diverse surfaces needs to be demonstrated to apply this concept on any kind of surface.

Considering the easiness and large-area scalability of cracked template metal network electrodes, we address the following questions in this work: 1) Is it possible to fabricate a metal network electrode on top of an organic layer by using a cracked template procedure to form a back electrode? 2) Can these metal network electrodes be combined as front as well as a back electrodes to realize ITO-free semitransparent solar cells for an organic photoactive layer? The main challenge here is to apply the cracked template approach on top of soluble organic layers without damaging the photoactive layer. This is very critical, as the cracked template needs to be removed by dissolution. We demonstrate for the first time that by a suitable adaptation of the cracked template method, Ag or Au back electrodes can be fabricated maintaining a transmittance of 80% for the whole visible range. To realize this, we first prepared Au network electrodes on top of PEDOT:PSS-coated glass and characterized these for determining the suitability for semitransparent solar cell fabrication. The fundamental properties of a metal network back electrode include haze, transmittance, and sheet resistance, and they are studied using a Au electrode as a typical example. We show that Ag and Au network electrodes can be integrated as front or back electrode depending on the device geometry and without influencing the photoactive layers. For realizing an ITO-free semitransparent solar cell, we chose a P3HT/$PC_{[61]}BM$ inverted geometry device. The solar cell characteristics of the ITO-free semitransparent solar cell are compared with those of a reference ITO/Ag opaque as well as ITO/Ag network devices. We realized an ITO-free semitransparent polymer solar cell with a PCE of 1.8% and a transmittance of 57% above 650 nm. These devices, having a Ag network on both sides do not exhibit any differences in performance in either back or front illumination mode. This research work mainly concerns with the relevant issues of electrode fabrication, and we have taken a typical reference photoactive layer (P3HT/$PC_{[61]}BM$) to demonstrate our concept. This is a general approach, which can be transferred to any kind of organic layer, material combination, and metal network as front or back electrode.

Results and Discussion

Fabrication of metal network electrode on PEDOT:PSS

The basic fabrication process flow for the metal network electrodes on top of PEDOT:PSS (≈50 nm) is schematically shown in Figure 1a. First the precursor dispersion was spin coated onto the PEDOT:PSS surface resulting in spontaneous formation of cracks during drying (Figure S1, Supporting Information). Interestingly, irrespective of the difference in the surface properties of the glass and PEDOT:PSS, the precursor dispersion cracks on both surfaces in a similar way. Moreover, crack grooves run down to the PEDOT:PSS surface, which is than filled in with Ag or Au by slow thermal evaporation (≈0.2 nm s^{-1}) in vacuum. The crackle layer is easily dissolved away by dipping in chloroform without affecting the PEDOT layer beneath. The lift-off procedure was also optimized using solvents such as ethyl acetate to adapt this template method for applications in solar cells. To study these metal electrodes on top of PEDOT:PSS, a Au metal network was selected as a typical example and several samples of different Au thicknesses in the range of 20–60 nm were prepared following the same procedure as discussed below.

A typical metal network electrode, Au (40 nm) network on PEDOT:PSS, was thoroughly characterized by a host of characterization techniques as shown in Figure 1. SEM images and its corresponding energy-dispersive spectroscopy (EDS) maps of the Au network fabricated on top of the PEDOT:PSS are shown in Figure 1b.

From the SEM image, it can be seen that the junctions of the network or web are well connected without any defects (Figure 1b). The Au network structures have a width from several hundreds of nm up to 5 μm and an average cell size (spacing between the grids) of 10–60 μm resulting in metal fill factor of approximately 12%. The metal network is continuous over large areas on the PEDOT:PSS layer (Figure S2, Supporting Information). The Au M, C K, and Si K signals in the EDS map reveal the presence of Au, C, and Si, respectively. As Au is fabricated directly on top of the PEDOT:PSS, the signal from the Au network is clearly visible and the C K signal is the inverse of Au K. This is due to the thickness of Au being more than the penetration depth of secondary electrons, which mask the PEDOT:PSS below it.

The signal from C K (red) arising from PEDOT:PSS is stronger in intensity than Si K (blue) arising from glass substrate, as expected to be the case. Moreover, the uniform dis-

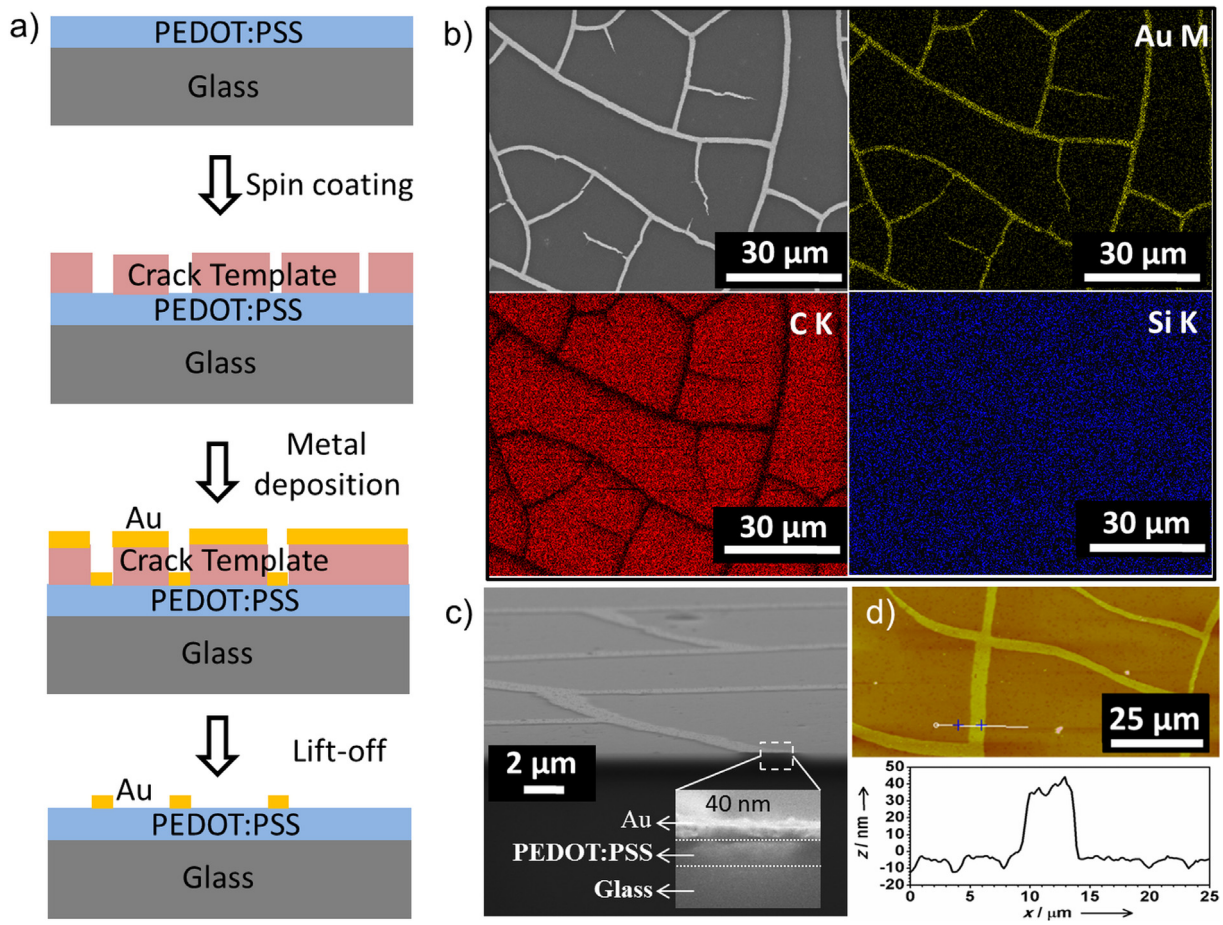

Figure 1. a) Schematic illustration of preparing a Au metal network electrode on PEDOT:PSS coated glass substrate by spin coating of the crack template, Au deposition and removal of crack template by lift-off. b) SEM image and corresponding EDS maps of Au M, C K, and Si K. c) SEM image showing the cross-sectional view and d) AFM image along with height profile of Au network on PEDOT:PSS layer.

tribution of C K signal in the void regions of the network shows that PEDOT:PSS is defect free even upon development of crack template by washing with organic solvents (Figure 1c). The Si K signal is much weaker, due to the presence of the approximately 50 nm PEDOT:PSS layer as seen from the cross-sectional image in Figure 1d. The good interfacial contact between the Au metal and PEDOT:PSS layer is crucial for efficient charge collection in devices. The atomic force microscopy (AFM) image and the corresponding height profile (Figure 1d) over the network electrode shows the smooth surface of PEDOT:PSS beneath the Au network. As seen from the AFM profile in Figure 1d, the average PEDOT:PSS roughness (R_a) is approximately 5 nm. The R_a of the Au network/PEDOT:PSS electrodes over entire $100\times100\ \mu m^2$ area is 9 nm, and the peak-to-valley roughness is 47 nm. As the metal fill factor per unit area is considerably low ($\approx12\%$), the overall roughness R_a is significantly reduced. The Ag and Au metal networks are very similar and therefore resemble in their properties considerably.

Optical and electrical properties of metal network electrode

The main properties of concern for a TCE are the optical transmittance, electrical conductivity, haze, and figure of merit (FOM), which gives the electrical/optical conductivity ratio. The electrodes fabricated in this way appear to be highly transparent as seen in Figure 2a. In this image, the letters behind the electrode indicates high optical transmission. The electrode exhibits a sheet resistance of approximately 3 Ω/□, which is significantly lower (by 3 orders of magnitude) as compared to the PEDOT:PSS that has resistance of approximately 1.5 kΩ/□. The uniformity in resistance is clearly observed in the homogeneous temperature distribution across the thermal image upon subjecting the electrode to a direct current (DC) bias of 6 V (Figure 2b). Electrothermal joule heating behavior through the transparent electrode is given in Figure S3 (Supporting Information).

The study of the optoelectronic properties for other electrodes with varying Au network thicknesses was conducted in detail. Figure 2c shows the optical transmission spectra over a broad spectral range corresponding to diffusive transmittance (T_D) with an average transmittance between 70–

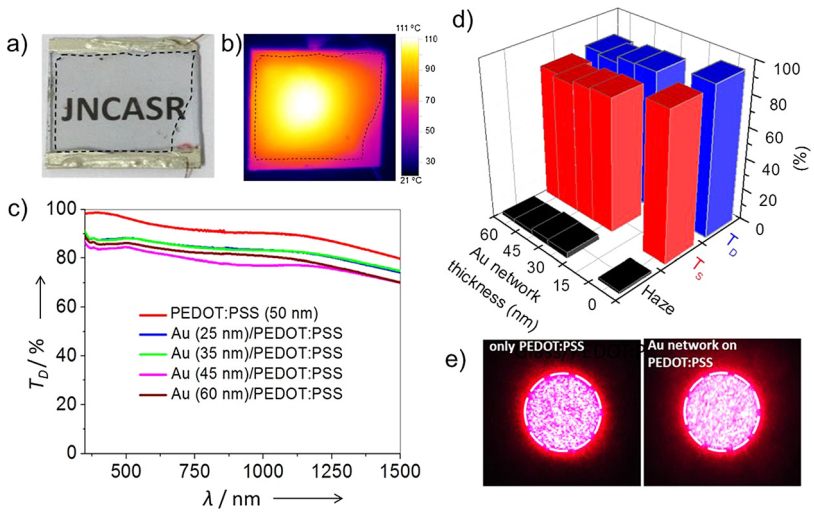

Figure 2. a) Digital photograph, b) thermal image (at 6 V DC bias) of a Au network on PEDOT:PSS, c) diffusive transmittance spectra (350–1500 nm) for various thicknesses, d) variation in T_S, T_D, and haze with Au network thickness, e) angular distribution of scattered light from PEDOT:PSS and Au network on PEDOT:PSS. Glass has been taken as reference for transmittance measurement.

85 %. The transmittance of the Au network/PEDOT:PSS electrodes is lowered by 10–15 % with respect to PEDOT:PSS thin film, which indicates that the network is highly transparent owing to low metal fill factor. The corresponding specular transmittance (T_S) spectra are shown in Figure S4 (Supporting Information).

Using average values of T_D and T_S as plotted in Figure 2d, the haze of the electrodes is calculated using the following relation: haze (%) = $(T_D - T_S/T_D)$. It refers to the percentage of light diffusely scattered through a transparent surface with respect to the total light transmitted. Haze is an important parameter to determine the optical visibility, especially for those applications where transparency is concerned. Interestingly, the electrodes exhibit an ultralow haze of approximately 5 % for metal thicknesses up to 60 nm. The angular distribution of the diffused light is seen in Figure 2e (see Figure S5 for details, Supporting Information). The narrow distribution of the spot shows that specular transmission dominates over diffusive component with an angular spread for the PEDOT:PSS layer and Au network/PEDOT:PSS electrode, approximately 0.3° and 0.5°, respectively (Figure 2e). These angular spread values can be lower than those of Ag NW derived TCEs.[28] The ultralow haze values for these electrodes are attributed to the extremely low fill factor and reduced surface roughness.

Figure S6 (Supporting Information) shows the interdependence between the transmittance (at 550 nm) and sheet resistance variation for different thicknesses of Au network on top of PEDOT:PSS. The overall resistance remains quite low with increasing transmittance for thinner layers, essentially overcoming the trade-off between the two counteracting properties. To evaluate this trade-off between the sheet resistance (R) and transmittance (T), the FOM is usually useful.[12] Therefore, the performance of these electrodes is further evaluated by specifying the commonly used FOM based on the electrical/optical conductivity ratio (σ_{DC}/σ_{OP}) calculated using following Equation (1)

$$\text{FOM}: \quad \sigma_{DC}/\sigma_{OP} = Z_O \Big/ 2R\left(T^{-1/2} - 1\right) \tag{1}$$

To achieve an R value of 10 Ω/□ and $T \approx 90\,\%$ requires $\sigma_{DC}/\sigma_{OP} \approx 350$. ITO electrodes having $T \approx 97\,\%$ and $R \approx 15$–30 Ω/□, exhibit FOM values of 400–800.[12] The FOM for our Au network (60 nm) on PEDOT:PSS is 765.

Solar Cell Preparation & Characterization

Three different solar cell configurations were prepared using the ITO/Ag opaque, ITO/network, and Ag/Ag network as front and back electrodes, respectively. The fabrication steps for a metal network back electrode on top of the photoactive material are schematically shown in Figure 3.

A polymer template layer was spin-coated onto PEDOT:PSS to form spontaneous cracks. After metal deposi-

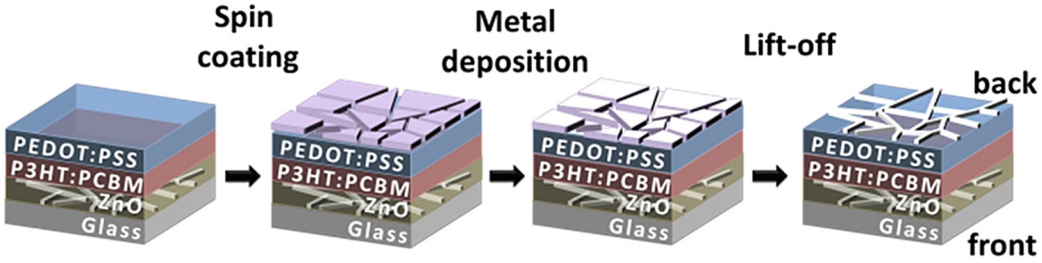

Figure 3. Schematics of process steps for the fabrication of ITO-free semitransparent polymer solar cell with a Ag/Ag network as front and back electrodes (glass/ZnO:Ag network/P3HT:PCBM/PEDOT:PSS/Ag network).

tion, the cracked template needed to be lifted-off by ultrasonication in suitable solvents. For the preparation of the front electrode on a glass substrate, the selection of solvent was not critical and we could use, for example, chloroform. But to remove the template as prepared on top of the photoactive layer coated with PEDOT:PSS, this procedure damaged the device. To find a suitable solvent that does not damage the device, different solvents were tested, and a reference device was ultra-sonicated in these solvents. It was determined that ultra-sonicating in ethyl acetate for 10 s removed the template completely and this treatment had no impact on the solar cell performance (Supporting Information, Figure S7).

For the purpose of comparison, all three of the devices using ITO/Ag opaque, ITO/Ag network, and Ag/Ag network as front and back electrodes were fabricated under the same conditions and for the same P3HT/$PC_{[61]}$BM thickness (Figure 4a). All of the front electrodes were coated with an optimum layer of ZnO to realize the inverted geometry.[27] To guarantee hole extraction/collection at the back electrode, the Ag network electrode was prepared on top of PEDOT:PSS. Both Ag und Au metal networks were tested as back electrodes. As an example, only the Ag network electrodes are discussed here (see Supporting Information for the results on Au network electrodes, Table S1 and Table S2).

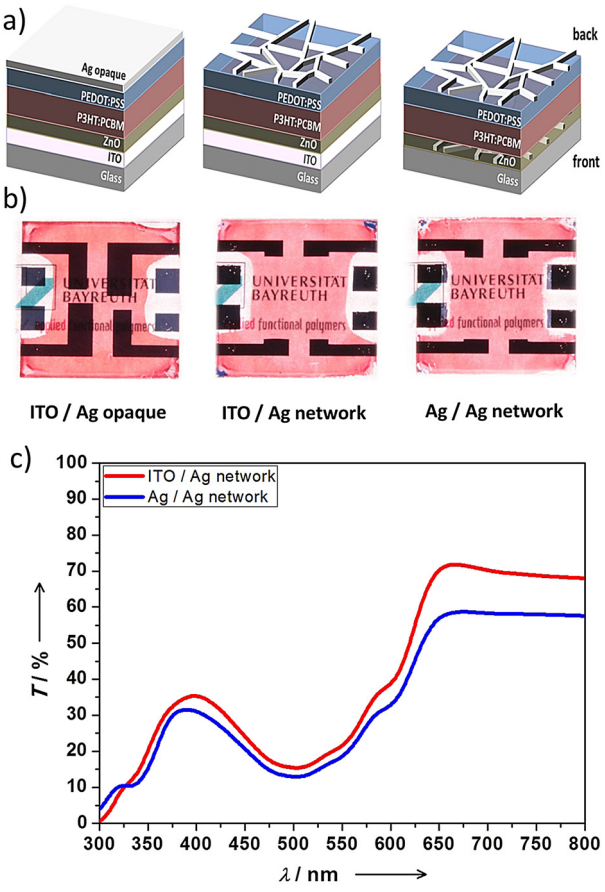

Figure 4. a) Schematics and b) photographs of all the devices studied: ITO/Ag opaque, ITO/Ag network, and the ITO-free semitransparent polymer solar cell with Ag/Ag network as front and back electrodes. c) Transmittance of complete devices with ZnO, P3HT/$PC_{[61]}$BM, and PEDOT:PSS for the ITO/Ag network and Ag/Ag network as front and back electrodes, respectively.

An optical micrograph of Ag/Ag network device (Figure S8, Supporting Information) clearly shows the formation of submicrometer network structures for both the front and back electrodes. Moreover the subsequent layer preparation and the fabrication of a Ag network on top of P3HT/$PC_{[61]}$BM layer have no detrimental effects on the underlying layers. It is clear from the photographs shown in Figure 4b that the letters behind the transparent solar cell are clearly visible and both the solar cells with ITO/Ag network and Ag/Ag network are similar in their semitransparency (Figure 4b). The transmittance spectra of the ITO/Ag network and Ag/Ag network devices are shown in Figure 4c.

The transmittance of the ITO/Ag network device is 15% at 500 nm (70% beyond 650 nm) whereas the Ag/Ag network device has a comparable transmittance of 13% at 500 nm (57% beyond 650 nm), which is slightly better than published results on Ag NW/PEDOT:PSS electrodes.[22] The low transmittance at 500 nm arises mainly from the intensive absorption of P3HT in this region for the layer thicknesses of approximately 180 nm used here. Further optimization of the P3HT layer thickness may be required to improve the transmittance without sacrificing much on performance. Further, the use of new photoactive materials that absorb in the near infrared with high transmittance in the visible region can result in improved semitransparent solar cells.

In this contribution, we were studying the consequences of integrating a metal network electrode on top of a typical organic layer to elucidate the general validity and feasibility of this approach to any kind of organic solar cell. Therefore, the semiconductor layer was not varied or optimized.

In the following, the photovoltaics parameters of all of the three types of devices are discussed in detail. Figure 5a shows the *J–V* characteristics of all three devices, which were measured under front illumination (see Figure S9 for back illumination curves, Supporting Information). The corresponding external quantum efficiency (EQE) spectra for both front and back illumination are given in Figure 5b. The respective values for the open-circuit voltage (V_{OC}), short-circuit current (J_{SC}), fill factor (*FF*), power conversion efficiency (PCE), series resistance (R_S), and shunt resistance (R_{SH}) are summarized in Table 1.

As seen in Figure 5, it is feasible to fabricate a metal network back electrode on top of a PEDOT:PSS-coated photoactive layer using the cracked template method described above to obtain considerably efficient photovoltaic devices. The back electrode fabrication is reproducible. The average values and standard derivation for a given number of solar cells are given in the Supporting Information (Table S3), and the data for the best devices are discussed here. All device parameters were obtained by illuminating the devices through a mask and the area of the device is defined by the mask as recommended for solar cell characterization.[29] In many of the published values, this is not the case, and therefore one has to be cautious in comparing the absolute values

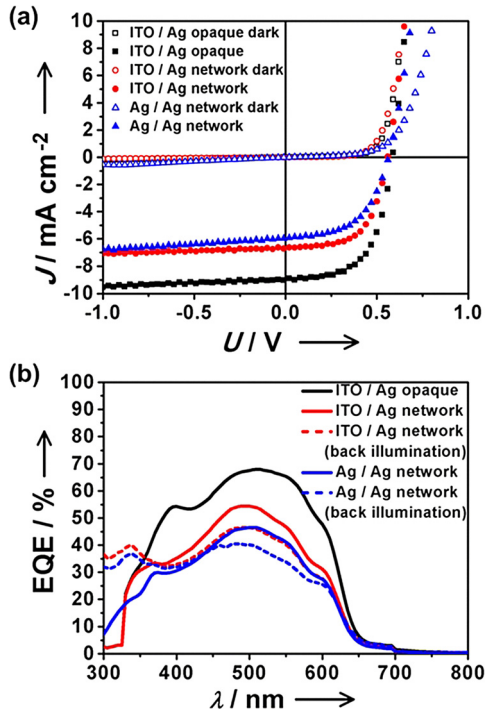

Figure 5. a) *J–V* characteristics in the dark (open symbols) and under light (filled symbols) and b) EQE under front and back illumination for all the three types of devices.

with those published in literature. In the Supporting Information (Figure S10 and Table S4), we have given the differences in solar cell parameters for the same device if measured correctly with a mask and without a mask, which is often practiced. A reference cell using ITO/Ag opaque exhibits 3.1% PCE here under standard conditions of measurement using a mask and without any artificial layer or additional back reflector. For comparison, the ITO/Ag network device shows 2.25% PCE whereas the Ag/Ag network devices exhibit 1.80% PCE. Thus the devices with the metal network as back electrode deliver less photocurrent compared to the ITO/Ag opaque reference device. This may be due to the lack of back reflection in the ITO/Ag network case and both lack of back reflection and decreased transmittance in the Ag/Ag network case. As expected, in the case of ITO/Ag network as well as Ag/Ag network devices, the lack of back reflection decreases the photocurrent as observed in Figure 5 (for reflection spectra of the solar cells please see Figure S11, Supporting Information). Additionally, the Ag/Ag network devices also have a small amount of loss in transmittance at the front electrode due to the thicker ZnO layers as well as Ag network. This observed effect on the front electrode is in agreement with what we observed in our previous work.[27]

The observed trend in photocurrent values agrees very well with the measured EQE. Additionally, we verified the effect of front and back illumination for both semitransparent solar cells having ITO/Ag network and the Ag/Ag network as front and back electrodes. For the *J–V* curves (back illumination data in Figure S8, Supporting Information) it does not matter, if the devices are illuminated from the front or back electrode. In the EQE curves, considerable differences are observed in the wavelength range of 300 to 400 nm. Interestingly for both the ITO/Ag network and Ag/Ag network devices in the case of front illumination, the EQE values between 300 and 400 nm are lower, whereas between 400 and 650 nm the EQE values are higher compared to back illumination. The lower EQE values between 300 and 400 nm are mainly due to optical losses at the front electrode arising from absorption of the glass/ITO/ZnO or glass/ZnO in the respective cases (compared to the Ag network in back illumination) upon illuminating from the front side.

To understand the resistance effects, the *J–V* characteristics under illumination for all of the three types of devices were analyzed to obtain R_S and R_{SH} near the open-circuit and short-circuit conditions respectively. All the devices have very low R_S ($<5\,\Omega\,cm^2$) and high R_{SH} values ($>1\,k\Omega\,cm^2$). This results in high *FF* values of 50–60%. The lower *FF* for Ag/Ag network devices correlates well with its highest R_S and lowest R_{SH} values. Thus, replacement of front ITO or back Ag opaque electrode with Ag network leads only to a very small increase in the overall R_S, with no considerable influence on R_{SH}.

Table 1. Summary of the solar cell parameters for the best devices corresponding to *J–V* characteristics shown in Figure 5a. Average values and standard derivations are given in Table S3 (Supporting Information).

Cathode/anode	V_{OC} [mV]	J_{SC} [mA cm^{-2}]	*FF* [%]	*PCE* [%]	$R_S@V_{OC}$ [Ω cm^2]	$R_{SH}@J_{SC}$ [kΩ cm^2]
ITO/Ag opaque	580	8.78	60.9	3.10	1.37	1.45
ITO/Ag network, front illumination	560	6.67	60.1	2.25	3.29	2.05
ITO/Ag network, back illumination	550	5.95	61.9	2.03	3.51	1.81
Ag/Ag network, front illumination	560	5.90	54.4	1.80	4.22	1.01
Ag/Ag network, back illumination	580	6.16	51.7	1.85	4.24	1.13

Conclusions

The concept of the fabrication of submicrometer metal network electrodes that are invisible to the naked eye using a cracked polymer template is successfully applied to the fabrication of a back electrode on top of a photoactive layer in a solar cell for the first time. Both Ag and Au network electrodes can be used as either front or back electrodes in a polymer solar cell to achieve ITO-free semitransparent devices. Here, the template process

is repeatedly applied before and after coating the photoactive layer. The biggest challenge of fabricating a transparent back electrode on top of an organic layer was achieved by optimization of the lift-off procedure for the template. Both the ITO/Ag network and Ag/Ag network devices exhibit considerably good efficiencies of approximately 2% PCE, which is comparable to any other semitransparent electrode system reported for P3HT/$PC_{[61]}BM$ blends. The method of cracked template is in principle scalable for large areas, and any kind of evaporable metal can be used in combination with this template approach. Further improvements in PCE and transmittance can be achieved by using other photoactive layers and by additional optimization of the layer thickness. In addition, this is a general approach to fabricate transparent metal electrodes on top of organic layers, where diverse material combination and type of metal can be used to realize different kinds of optoelectronic devices.

Experimental Section

Fabrication of Ag or Au network by cracked template method on PEDOT:PSS

For the fabrication of metal network electrodes on PEDOT:PSS, we modified the published procedure for a cracked template method on glass.[27] Glass substrates were washed and ultrasonicated in water, acetone, and isopropyl alcohol (IPA), respectively. The substrates were dried using a N_2 gun before use. In the second step, a commercially available acrylic resin nanoparticle dispersion (Ming Ni Cosmetics Co., Guangzhou, China) was diluted to achieve a well-dispersed solution of 0.6 g mL^{-1} concentration using a commercially available diluter (Ming Ni Cosmetics Co., Guangzhou, China). The diluted dispersion was spin coated onto a PEDOT:PSS coated glass substrate at 1000 rpm for 120 s. During drying, this film developed cracks suitable to be used as a template. In the next step, Ag or Au metal was deposited using a thermal evaporator (BOC Edwards, Auto 306, FL 400 and Hind High Vacuum Co., India). In the final step, the cracked template was removed by dissolving in either chloroform or acetone or ethyl acetate.

Solar cell fabrication and characterization

The reference solar cell, ITO/ZnO/P3HT:$PC_{[61]}BM$/PEDOT:PSS/Ag opaque having an inverted geometry was prepared according to the published procedures.[27] The only difference was the use of structured ITO here. For realizing the devices with ITO as front electrode and Ag or Au network as back electrode, a similar procedure was adopted up to the PEDOT:PSS layer preparation. For the back metal network electrode, the polymer crack template was prepared on the PEDOT:PSS (Clevios HTL Solar) layer as described above, followed by 100 nm metal (Ag or Au) deposition using a thermal evaporator (BOC Edwards, Auto 306, FL 400). The polymer lift-off was performed by ultra-sonication of the entire device in ethyl acetate for 10 s. To realize the semitransparent ITO-free device with Ag network as both front and back electrodes, the published procedure[27] for the front electrode was modified to structure the metal network area using masks, and it was combined with the newly adopted method for the back electrode preparation. The average area of the devices was in the range of 4–9 mm^2 as defined by the area of the light mask. Current–voltage characteristics were measured under N_2 atmosphere using suitable masks under standard AM1.5 G spectral conditions at an intensity of 100 mW cm^{-2} using a solar simulator (Newport-Oriel, 92250A-1000) and an electrometer (Keithley, Model 6517). The light source was regularly calibrated using a silicon solar cell (WPVS cell, ISE Call lab, Freiburg). Near-normal reflectance spectra of full solar cells were obtained using an integrating sphere in a Bentham PVE300 photovoltaic characterization system. External quantum efficiencies were measured using the same Bentham PVE300 photovoltaic device characterization system. For the simplicity of discussion of results, the best solar cell parameters are given. However average values and the standard derivation for a large number of devices are given in the Supporting Information.

Other characterization methods

SEM was performed using a Nova NanoSEM 600 instrument (FEI Co., The Netherlands). Energy-dispersive spectroscopy (EDS) mapping was performed using an energy-dispersive X-ray analysis (EDAX) Genesis instrument (Mahwah, NJ) attached to the SEM column. AFM measurements were performed using di Innova (Bruker, USA) in contact mode. Standard Si cantilevers were used for normal topography imaging. Wyko NT9100 Optical Profiling System (Bruker, USA) was used for height and depth measurements and Dektak profiler for thickness measurements. A PerkinElmer Lambda 900 UV/visible/near-IR spectrometer was used to perform the transmission and haze measurements of electrodes and device.

Acknowledgements

The financial support from the EU Project "Largecells" (Grant No. 261936), Department of Science and Technology, Government of India, DFG (SFB 840) and the Bavarian State Ministry of Science, Research, and Arts for the collaborative Research Network "Solar Technologies go Hybrid" is gratefully acknowledged. K.D.M.R. thanks UGC for the SRF fellowship and C.H. acknowledges financial support from DFG (GRK 1640) and help in instrumentation and software from Jonas Mayer, University of Bayreuth.

Keywords: ITO-free · organic solar cell · photovoltaics · silver · transparent conducting electrode

[1] G. Li, R. Zhu, Y. Yang, *Nat. Photonics* **2012**, *6*, 153–161.
[2] R. Søndergaard, M. Hösel, D. Angmo, T. T. Larsen-Olsen, F. C. Krebs, *Mater. Today* **2012**, *15*, 36–49.
[3] W. Li, W. S. C. Roelofs, M. Turbiez, M. M. Wienk, R. A. J. Janssen, *Adv. Mater.* **2014**, *26*, 3304–3309.
[4] T. Xu, L. Yu, *Mater. Today* **2014**, *17*, 11–15.
[5] M. Kaltenbrunner, M. S. White, E. D. Głowacki, T. Sekitani, T. Someya, N. S. Sariciftci, S. Bauer, *Nat. Commun.* **2012**, *3*, 770.
[6] H. Kim, C. M. Gilmore, A. Pique, J. S. Horwitz, H. Mattoussi, H. Murata, Z. H. Kafafi, D. B. Chrisey, *J. Appl. Phys.* **1999**, *86*, 6451–6461.
[7] A. Kumar, C. Zhou, *ACS Nano* **2010**, *4*, 11–14.
[8] D. R. Cairns, R. P. Witte, D. K. Sparacin, S. M. Sachsman, D. C. Paine, G. P. Crawford, R. R. Newton, *Appl. Phys. Lett.* **2000**, *76*, 1425–1427.

[9] S. Bae, H. Kim, Y. Lee, X. Xu, J.-S. Park, Y. Zheng, J. Balakrishnan, T. Lei, H. R. Kim, Y. I. Song, Y.-J. Kim, K. S. Kim, B. Özyilmaz, J.-H. Ahn, B. H. Hong, S. Iijima, *Nat. Nanotechnol.* **2010**, *5*, 574–578.
[10] R. C. Tenent, T. M. Barnes, J. D. Bergeson, A. J. Ferguson, B. To, L. M. Gedvilas, M. J. Heben, J. L. Blackburn, *Adv. Mater.* **2009**, *21*, 3210–3216.
[11] H. Z. Geng, K. K. Kim, K. P. So, Y. S. Lee, Y. Chang, Y. H. Lee, *J. Am. Chem. Soc.* **2007**, *129*, 7758–7759.
[12] S. De, T. M. Higgins, P. E. Lyons, E. M. Doherty, P. N. Nirmalraj, W. J. Blau, J. J. Boland, J. N. Coleman, *ACS Nano* **2009**, *3*, 1767–1774.
[13] D. Kim, L. Zhu, D. J. Jeong, K. Chun, Y. Y. Bang, S. R. Kim, J. H. Kim, S. K. Oh, *Carbon* **2013**, *63*, 530–536.
[14] Y. Galagan, J.-E. J. M. Rubingh, R. Andriessen, C.-C. Fan, P. W. M. Blom, S. C. Veenstra, J. M. Kroon, *Solar Energy Mater. Solar Cells* **2011**, *95*, 1339–1343.
[15] Y. Galagan, B. Zimmermann, E. W. C. Coenen, M. Jørgensen, D. M. Tanenbaum, F. C. Krebs, H. Gorter, S. Sabik, L. H. Slooff, S. C. Veenstra, J. M. Kroon, R. Andriessen, *Adv. Energy Mater.* **2012**, *2*, 103–110.
[16] J. E. Carlé, M. Helgesen, M. V. Madsen, E. Bundgaard, F. C. Krebs, *J. Mater. Chem. C* **2014**, *2*, 1290–1297.
[17] a) J. Lee, P. Lee, H. Lee, D. Lee, S. S. Lee, S. H. Ko, *Nanoscale* **2012**, *4*, 6408–6414; b) W. Gaynor, G. F. Burkhard, M. D. McGehee, P. Peumans, *Adv. Mater.* **2011**, *23*, 2905–2910.
[18] M. Reinhard, R. Eckstein, A. Slobodskyy, U. Lemmer, A. Colsmann, *Org. Electron.* **2013**, *14*, 273–277.
[19] K. Zilberberg, F. Gasse, R. Pagui, A. Polywka, A. Behrendt, S. Trost, R. Heiderhoff, P. Görrn, T. Riedl, *Adv. Funct. Mater.* **2014**, *24*, 1671–1678.
[20] K.-S. Chen, J.-F. Salinas, H.-L. Yip, L. Huo, J. Hou, A. K.-Y. Jen, *Energy Environ. Sci.* **2012**, *5*, 9551–9557.
[21] S. K. Hau, H.-L. Yip, J. Zoua, A. K.-Y. Jen, *Org. Electron.* **2009**, *10*, 1401–1407.
[22] J. H. Yim, S.-Y. Joe, C. Pang, K. M. Lee, H. Jeong, J.-Y. Park, Y. H. Ahn, J. C. de Mello, S. Lee, *ACS Nano* **2014**, *8*, 2857–2863.
[23] F. Guo, X. Zhu, K. Forberich, J. Krantz, T. Stubhan, M. Salinas, M. Halik, S. Spallek, B. Butz, E. Spiecker, T. Ameri, N. Li, P. Kubis, D. M. Guldi, G. J. Matt, C. J. Brabec, *Adv. Energy Mater.* **2013**, *3*, 1062–1067.
[24] F. Guo, P. Kubis, T. Stubhan, N. Li, D. Baran, T. Przybilla, E. Spiecker, K. Forberich, C. J. Brabec, *ACS Appl. Mater. Interfaces* **2014**, *6*, 18251–18257.
[25] B. Han, K. Pei, Y. Huang, X. Zhang, Q. Rong, Q. Lin, Y. Guo, T. Sun, C. Guo, D. Carnahan, M. Giersig, Y. Wang, J. Gao, Z. Ren, K. Kempa, *Adv. Mater.* **2014**, *26*, 873–877.
[26] a) K. D. M. Rao, R. Gupta, G. U. Kulkarni, *Adv. Mater. Interfaces* **2014**, *1*, 1400090; b) S. Kiruthika, R. Gupta, K. D. M. Rao, S. Chakraborthy, N. Padmavathy, G. U. Kulkarni, *J. Mater. Chem. C* **2014**, *2*, 2089–2094.
[27] K. D. M. Rao, C. Hunger, R. Gupta, G. U. Kulkarni, M. Thelakkat, *Phys. Chem. Chem. Phys.* **2014**, *16*, 15107–15110.
[28] C. Preston, Z. Fang, J. Murray, H. Zhu, J. Dai, J. N. Munday, L. Hu, *J. Mater. Chem. C* **2014**, *2*, 1248–1254.
[29] S. A. Gevorgyan, J. E. Carlé, R. Søndergaard, T. T. Larsen-Olsen, M. Jørgensen, F. C. Krebs, *Solar Energy Mater. Solar Cells* **2013**, *110*, 24–35.

Received: January 13, 2015
Revised: March 5, 2015
Published online on May 5, 2015

